Front. Earth Sci. 2021, 15(2): 471–489
https://doi.org/10.1007/s11707-020-0851-z

RESEARCH ARTICLE

# Physical-property cutoffs of tight reservoirs by field and laboratory experiments: a case study from Chang 6, 8–9 in Ordos Basin

**Bingbing SHI[1], Xiangchun CHANG (✉)[1,2], Zhongquan LIU[3], Ye LIU[1], Tianchen GE[1], Pengfei ZHANG[1], Yongrui WANG[1], Yue WANG[1], Lixin MAO[1,4]**

1 College of Earth Science and Engineering, Shandong University of Science and Technology, Qingdao 266590, China
2 Laboratory for Marine Mineral Resources, Pilot National Laboratory for Marine Science and Technology, Qingdao 266071, China
3 Petroleum Exploration and Development Research Institute, Shengli Oilfield Company of SINOPEC, Dongying 257015, China
4 Jiangsu Design Institute of Geology for Mineral Resources, Xuzhou 221006, China



**Abstract** Tight sandstone reservoirs are generally characterized by complex reservoir quality, non-Darcy flow, and strong heterogeneity. Approaches utilized for evaluating physical property cutoffs of conventional reservoirs maybe inapplicable. Thus, a comprehensive investigation on physical property cutoffs of tight sandstone reservoirs is crucial for the reserve evaluation and successful exploration. In this study, a set of evaluation approaches take advantage of field operations (i.e., core drilling, oil testing, and wireline well logging data), and simulation experiments (i.e., high-pressure mercury injection-capillary pressure (MICP) experiment, oil-water relative permeability experiment, nuclear magnetic resonance (NMR) experiment, and biaxial pressure simulation experiment) were comparatively optimized to determine the physical property cutoffs of effective reservoirs in the Upper Triassic Chang 6, Chang 8 and Chang 9 oil layers of the Zhenjing Block. The results show that the porosity cutoffs of the Chang 6, Chang 8, and Chang 9 oil layers are 7.9%, 6.4%, and 8.6%, and the corresponding permeability are 0.08 mD, 0.05 mD, and 0.09 mD, respectively. Coupled with wireline well logging, mud logging, and oil testing, the cut-off of the thickness of single-layer effective reservoirs are approximately 3.0 m, 3.0 m, and 2.0 m, respectively. Depending on the cutoffs of critical properties, a superimposed map showing the planar distribution of the prospective targets can be mapped, which may delineate the effective boundary of prospective targets for petroleum exploration of tight sandstone reservoirs.

**Keywords** tight sandstone reservoirs, cutoffs of petrophysical property, field operations, simulation experiments, Yanchang Formation, Ordos Basin

## 1 Introduction

With advances in oil and gas exploration technology, tight sandstone deposits have manifested great potential for extraction (Law and Curtis, 2002; Makhloufi et al., 2013; Yang et al., 2013; Wang et al., 2017a; Cui et al., 2019; Li et al., 2019c; Pang et al., 2019, 2020a and 2020b). By the end of 2016, China's established continental tight oil production capacity reached $1.553 \times 10^6$ tons (Hu et al., 2018). With the deepening exploitation of tight sandstone reservoirs, the physical property cut-off of the exploitation is gradually decreased to the critical conditions of the oil charging. And it is becoming increasingly important for the accurate determination of the physical property cut-off of the tight sandstone reservoirs. Tight sandstone reservoirs are widely developed in the Upper Triassic Yanchang ($T_3y$) Formation of the Zhenjing Block (Chang 6, Chang 8, and Chang 9 oil layers), south-western Ordos Basin. Previously, numerous successful studies have been conducted on the Yanchang Formation, which effectively guided the exploration and development of tight sandstone reservoirs (Liu et al., 2013; Li et al., 2017a, 2017b and 2019a; Wang et al., 2017a and 2017b; Yang et al., 2017; Shi et al., 2019 and 2020a; Liu et al., 2020a). However, previous

Received July 10, 2020; accepted November 18, 2020

E-mails: xcchang@sdust.edu.cn; xcchang@sina.com

researches of tight oil reservoirs primarily focus on the reservoir densification process, physical properties, fluid seepage characteristics, macroscopic pore geometries, and the distribution law of tight reservoirs, especially on the cutoffs of petrophysical properties (Worthington, 2008 and 2010; Masoudi et al., 2014; Worthington and Majid, 2014; Wang et al., 2015a; Gong et al., 2016; Zhou et al., 2016; Rostami et al., 2019; Li et al., 2019b and 2020; Zheng et al., 2020).

In recent years, research approaches for determining physical property cutoffs of conventional reservoirs have widely been investigated, various sets of approaches were proposed including physical properties, field operations (i.e., core drilling, oil testing, and wireline well logging data), and simulation experiments (i.e., high-pressure mercury injection capillary pressure (MICP) experiment, oil-water relative permeability experiment, nuclear magnetic resonance (NMR) experiment, stress sensitivity experiment, and biaxial pressure simulation experiment), and based on dynamic mechanism of tight oil reservoir accumulation to distinguish the cutoffs of the petrophysical properties of conventional reservoirs. (Hohn, 1989; Kikani and Pedros, 1991; Pittman, 1992; David et al., 1994; Wan et al., 1999; Wei et al., 2005; Worthington and Cosentino, 2005; Peng et al., 2009).

Besides, the upper limits of petrophysical parameters have been found to be consistent (porosity $< 10\%$ and overburden matrix permeability $< 0.1$ mD; Holditch, 2006; Aguilera, 2014; Zou et al., 2009 and 2012a). However, an issue directly related to the exploration and development of tight sandstone reservoirs remains in that the cutoffs of tight sandstone reservoirs has not been clearly understood thus far. Therefore, a universally approach that is more accurate, in accordance with the actual formation conditions, and considers the economic benefits to calculate the cut-offs of petrophysical property of tight sandstone reservoirs is lacking. With the extensive research on the micro-pore structure and seepage characteristics of tight sandstone reservoirs, conventional and distinct research approaches have highlighted numerous problems in the characterization of tight sandstone reservoirs (Masters, 1979; Gies, 1984; Wang et al., 2008; Dai et al., 2012; Zou et al., 2012a and 2012b; Baytok and Pranter, 2013; Jia et al., 2016; Guo et al., 2017; Qiu et al., 2017; Tan et al., 2017; Liu et al., 2020b). With the gradual densification of tight sandstone reservoirs under the deep-burial condition, tight reservoirs developed unique pore structure and fluid seepage characteristics. Thus, several approaches mentioned above for determining the cutoffs of conventional reservoirs maybe inapplicable to the evaluation of tight sandstone reservoirs (Shi et al., 2015).

In this study, in the consideration of the characteristics of complex reservoir quality, non-Darcy flow, strong heterogeneity, and micro-pore throats of tight sandstone reservoirs, using the preferred approaches for comprehensive delineated the cutoffs of tight sandstone reservoirs. Combined with the cut-off of the thickness of single-layer effective reservoirs, we obtain a congruent map showing the planar distribution of prospective targets, which may delineate the effective boundary of prospective targets for petroleum exploration of tight sandstone reservoirs. The preferred approaches are of profound significance for resource evaluations of tight oil reservoirs and the selection of exploration zones.

## 2 Geological settings

The Zhenjing Block is situated in the southern part of the Tianhuan Depression, south-western Ordos Basin, China (Fig. 1(a)), which is in the transition area between the north-westward depression and its south-western nose-shaped uplift. The isopach map showing the top of $T_3y$ Formation is featured by structural west high and east low (Fig. 1(b)).

The $T_3y$ Formation, deposited from the Carnian stage to the Norian stage, is subdivided into 10 intervals from bottom to top (Chang 10 to Chang 1), but wireline well logging data show that the Chang 3 and Chang $4 + 5$ layers are generally missing in the study area. All the intervals consist of sandstones, mudstones, and shales, among which the Chang 7 oil layer is composed predominantly of oil shales and black mudstones; the other intervals are composed of sandstones and mudstones (Fig. 2(a)). Therefore, Chang 7 oil layer serves as the source rock and seal for the underlying Chang 9 and Chang 8 and overlying Chang 6 oil layers. Chang 6, Chang 8, and Chang 9 oil layers have been identified as important exploration targets, and important progress has been made in exploration in recent years (Fu et al., 2014). At present, up to $18005 \times 10^4$ tons of proven oil reserves have been identified in the Zhenjing Block. Specifically, proven oil reserves of the Chang 6, Chang 8, and Chang 9 oil layers account for 99.0%, and the others account for only 1.00% ($147.7 \times 10^4$ tons), revealing that the Chang 6, Chang 8, and Chang 9 oil layers are main oil-producing horizons of the Zhenjing Block. The proven oil reserves of the Chang 8, Chang 9, and Chang 6 oil layers are $14211 \times 10^4$ tons, $3645 \times 10^4$ tons, and $356 \times 10^4$ tons, respectively, accounting for 79.0%, 18.0%, and 2.0% (Fig. 2(b)).

Sandstones are classified according to the method of Folk et al. (1970). Based on the analysis of rock slices of 30-seven wells in the study area (Fig. 3(a)), from Chang 6, Chang 8 to Chang 9, the contents of quartz decreased from 60.9% to 32.6% on average, contents of feldspar and rock fragments increased from 39.1% to 67.4% on average, and corresponding average composition of the framework grains from $Q_{60.9}F_{22.0}R_{17.1}$ to $Q_{32.6}F_{39.3}R_{28.1}$. As showed in Fig. 3(b), with increasing depth, the contents of volcanic rock fragments increased and metamorphic rock fragments decreased.

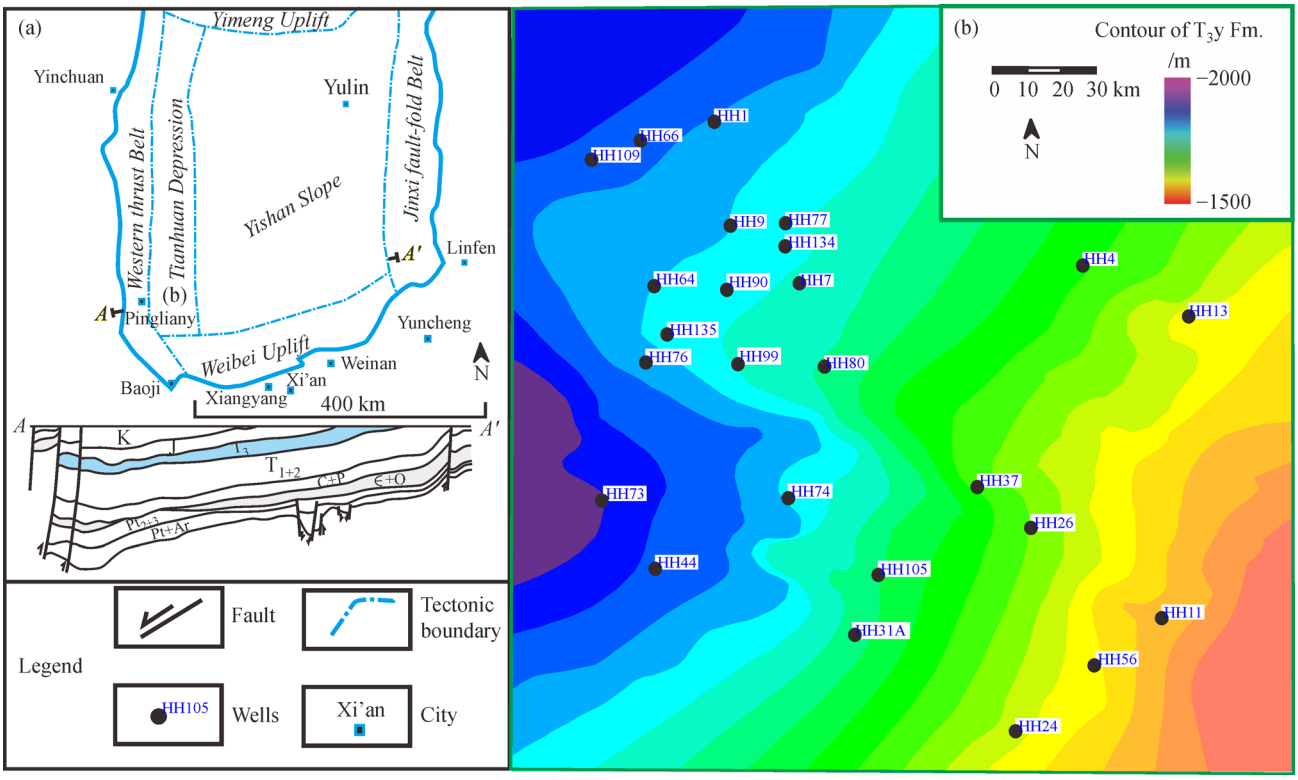


**Fig. 1** (a) Regional location and (b) isoline showing the top of Yanchang Formation of the Zhenjing Block, Ordos Basin.

## 3 Sample selection and experiments

### 3.1 Samples preparations and materials

In this study, the core samples, wireline well logging, oil testing data of the Chang 6, Chang 8, and Chang 9 oil layers of 25 wells in the Zhenjing Block were collected from the SINOPEC Petroleum Exploration and Production Research Institute, Beijing. All samples used in this study were taken from more than 270 m well cores and 1220 thin sections of the 25 wells at the depths of 1781–2172 m in the Zhenjing Block were observed (Fig. 1(b)).

### 3.2 Petrophysical property analysis

The samples were collected for porosity and permeability testing using cylinders of 2.5 cm diameter and 5 cm length (the relevant petrophysical property data used in this study can be seen in Supplementary data). All the cylinders were drilled along the horizontal direction of the cores. Porosity was measured on a JS100007 helium porosimeter and permeability was measured on an A-10133 gas permeameter using standard industry methods. Both the helium porosimeter and gas permeameter were manufactured by Micromeritics Instrument (Shanghai) Ltd.

### 3.3 Grain-size analysis

The compositions of the Chang 6, Chang 8, and Chang 9 sandstones were determined by point counts of at least 200 grains per thin section. Grain sizes were measured from the photomicrographs of thin sections using Image-Pro Plus software (Media Cybernetics), with the manual function, and each of the photomicrographs had at least 160 grains.

### 3.4 Simulation experiments

In this study, an integration of stress sensitivity analysis, high-pressure mercury injection capillary pressure (MICP) experiment, oil-water relative permeability test, and nuclear magnetic resonance (NMR) experiment, together with biaxial pressure simulation experiment were analyzed for determining the cutoffs of petrophysical property of tight sandstone reservoir.

Stress sensitivity analysis of 13 core samples was conducted using a PoroPDP-200 type instrument to measure porosity and permeability by the pulse method under overburden stress, according to the requirements of the industry standard for stress sensitivity experiment (SY/T5358-2002,≥1mD). The gas employed for the porosity

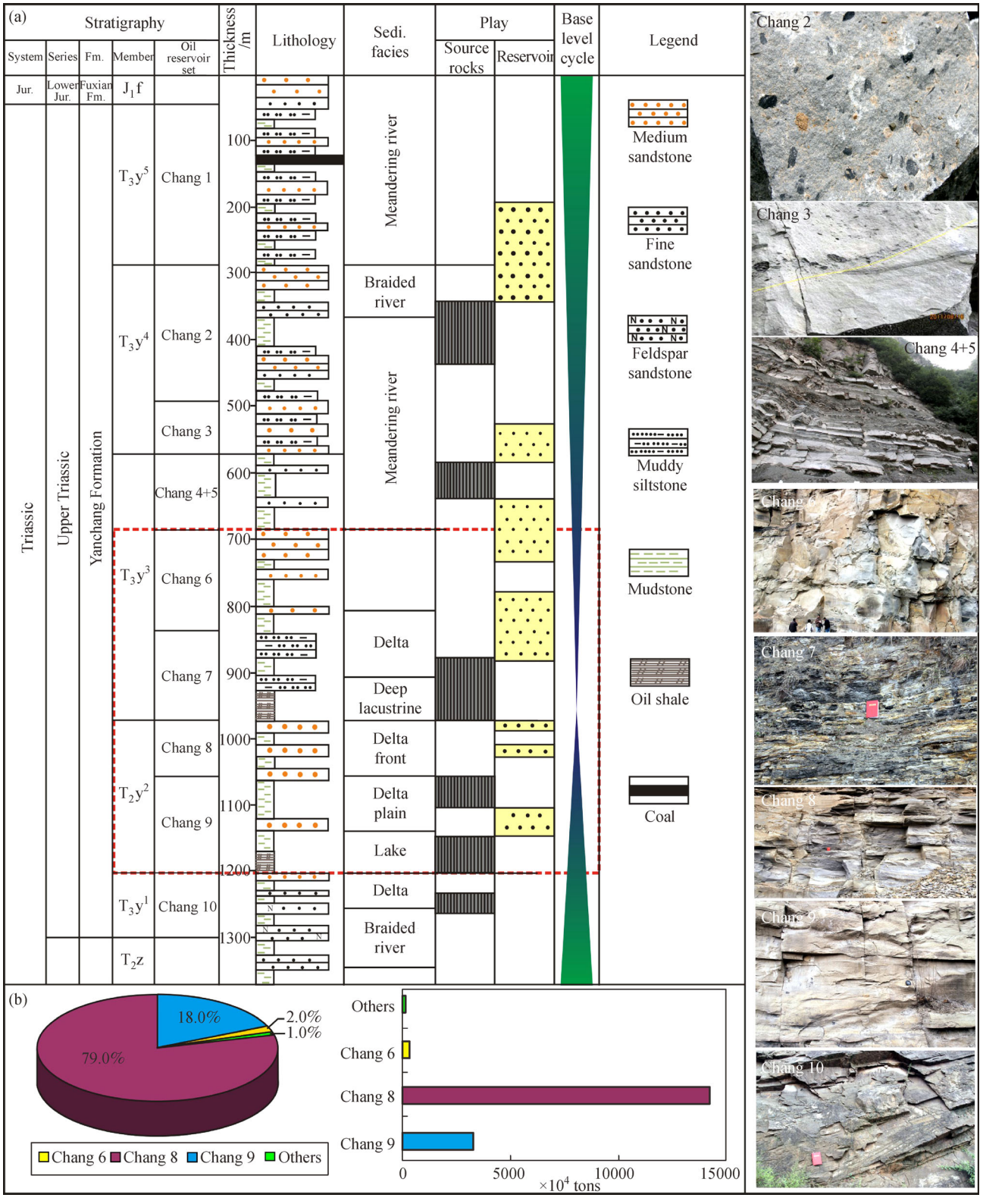


**Fig. 2** Comprehensive (a) stratigraphic column and (b) pie chart of abundance of reserves of the Chang 6, Chang 8 and Chang 9 oil layers of the Zhenjing Block, Ordos Basin. Notes: $T_3y$: Upper Triassic Yanchang Formation; $J_{1–2}y$: Lower to Middle Jurassic Yan'an Formation.

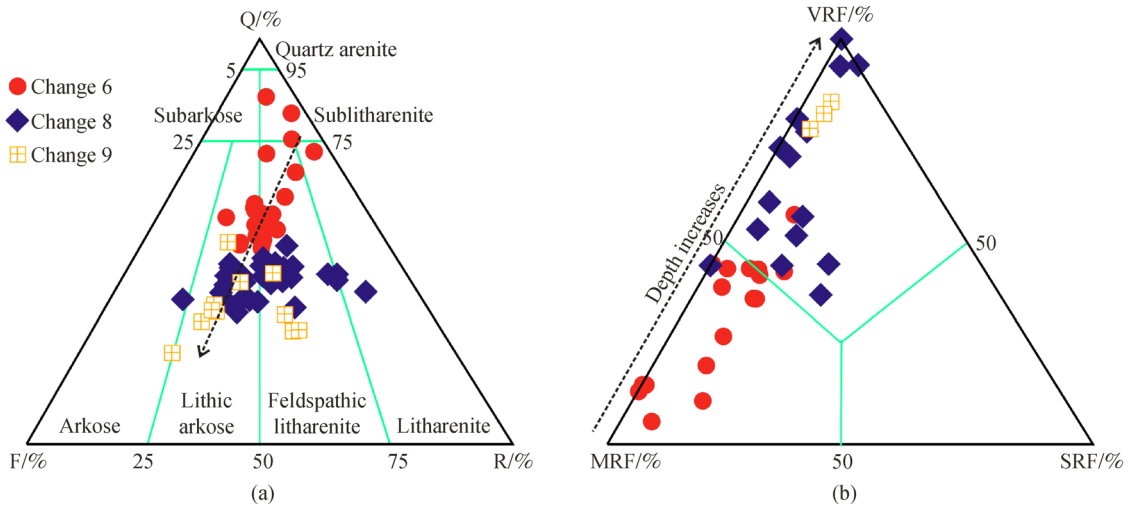


**Fig. 3** Ternary diagram showing the (a) framework compositions and (b) detrital components of the Chang 6, Chang 8 and Chang 9 tight sandstones in the Zhenjing Block. Notes: Q: quartz; F: feldspar; RF: rock fragments; VRF: volcanic rock fragments; MRF: metamorphic rock fragments; SRF: sedimentary rock fragments.

test was helium and, for the permeability test, nitrogen. When measuring permeability, the overburden stress was initiated at 0.0 MPa and gradually increased until the confining pressure was maximized at 55.0 MPa. The overburden stress was later gradually reduced.

The MICP experiment was conducted on 218 samples from 24 wells using a Pore Sizer 9320 mercury porosimeter manufactured by Micromeritics Instrument (Shanghai) Ltd. to confirm pore-throat radius and displacement pressure.

The unsteady-state displacement approach was utilized to determine the oil-water relative permeability (Esmaeili et al., 2019; Wang et al., 2015b and 2019). An immiscible displacing fluid (formation water with a salinity of 85000 mg/L) was injected at a constant rate to replace crude oil (viscosity of 2.80 mPa·s) in situ to the highest possible saturation in core samples in the laboratory. The transient behavior of the pressure drop across the length of the core and the volumes of the produced phases were recorded periodically, and the oil-water relative permeability characteristics were inferred from the recorded production and pressure drop history of the displacement test.

NMR measurements combined with centrifugal experiments were performed using a UNIQ PMR nuclear magnetic resonance analyzer (Beijing Yongshengtong Technology Development Co., Ltd.) to obtain the transverse relaxation time ($T_2$) spectrum of nine wells. Samples were collected every 0.30–0.50 m for intervals with oil and gas, and samples were collected every 0.50 m for intervals without oil and gas. First, the NMR measurements of nine wells were performed on samples in the fully water-saturated state (brine with 41000 ppm). Then, the movable water in the samples was centrifuged by a centrifuge machine and the NMR measurements were performed in the irreducible water state. The centrifugal pressure was set up as 600psi for tight sandstone samples, and the duration was set up as one hour. In the NMR experiment, the saturation of the movable fluid is utilized to calculate the porosity ($\varphi_{nmr}$), and the permeability ($K_{nmr}$) is obtained using the following Eq. (1) (Adebayo et al., 2020; Zhang et al., 2020).

$$K_{nmr} = C \cdot \varphi_{nmr}^2 \cdot T_2^2, \quad (1)$$

where $K_{nmr}$: cuttings permeability, mD; $\varphi_{nmr}$: cuttings porosity, %; $C$: 0.5.

Liu et al. (2012a and 2012b) proposed a biaxial pressure simulation experiment to study the critical conditions of the oil charge (Fig. 4(a)). In this study, 34 core samples of the Chang 6 and Chang 8 oil layers were prepared as cylindrical rock plugs of 2.5 cm diameter and 4–6 cm length. For the simulated formation fluids, a saturated solution of NaCl with a salinity of 49600 × $10^{-3}$ mg/L and T60 lubricant with a resistivity of 0.1368 Ω·m (25°C) and a relatively high viscosity were used. By exerting confining pressure ($\sigma_1$) and axial pressure ($\sigma_2$) on the core samples to simulate its stress state under different burial-depth conditions, the simulated formation fluid was charged into the cores to simulate the oil charging process (Fig. 4(b)). After charging the simulated formation fluid, the resistivity value monitored by the RLC bridge increased dramatically. In this study, the preliminary value of $\sigma_1$ was 5 MPa, and a set of minimum charging

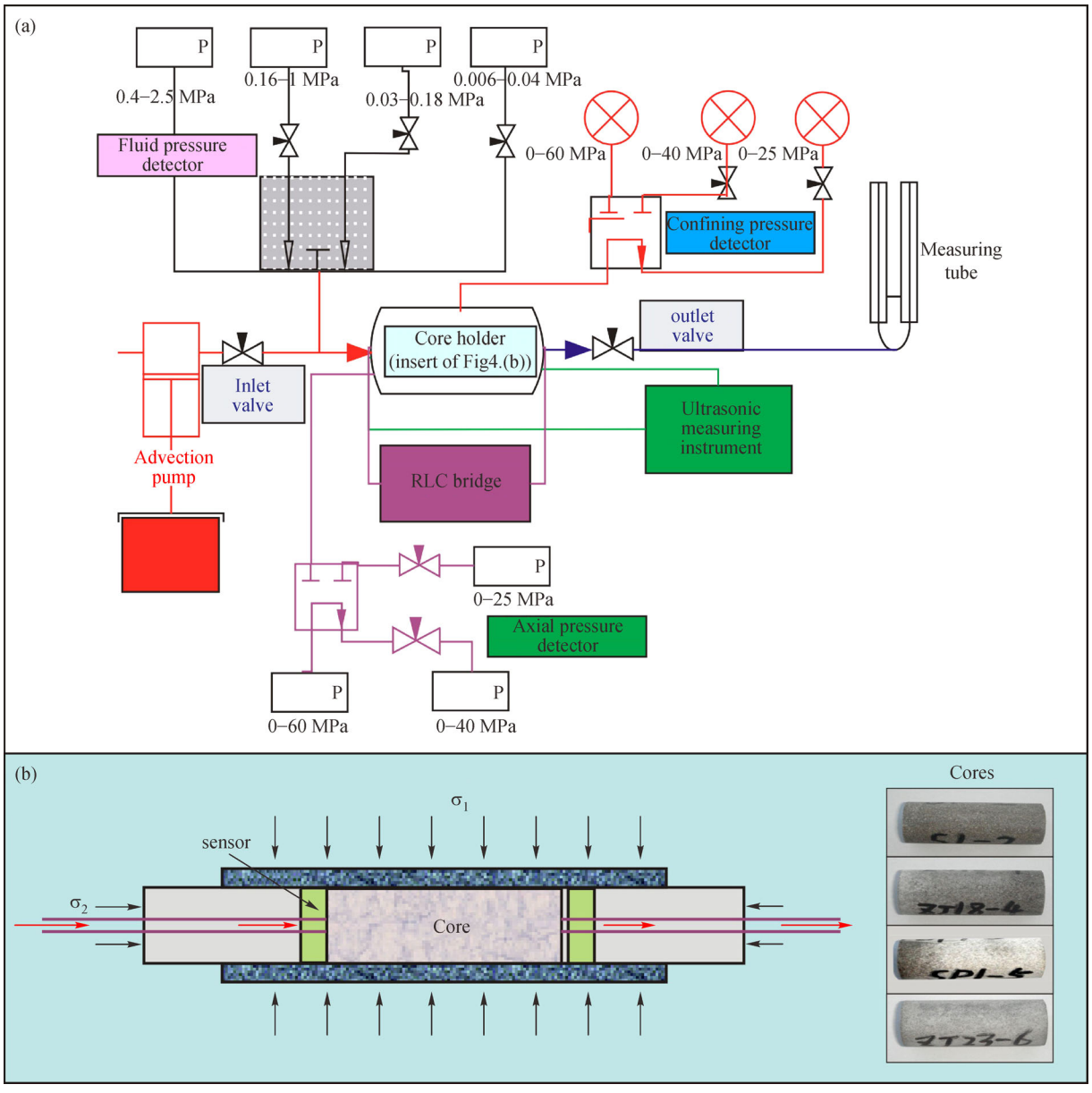


**Fig. 4** Experimental apparatus for biaxial pressure simulation experiment. Notes: $\sigma_1$: confining pressure; $\sigma_2$: axial pressure (modified after Liu et al., 2012a and 2012b).

pressure values was monitored for each increase in $\sigma_1$ (simulated burial-depth increase). In theory, 8 sets of data can be collected when the confining pressure is increased to a maximum of $\sigma_1$ (40 MPa). $\sigma_2$ is determined using Eq. (2) (Liu et al., 2012a and 2012b):

$$\sigma_2 = \sigma_1 \times \gamma/(1-\gamma), \quad (2)$$

where $\sigma_1$: confining pressure, MPa; $\sigma_2$: axial pressure, MPa; $\gamma$: dynamic Poisson ratio.

## 4 Results and discussion

### 4.1 Inapplicability of determining the cut-off of the tight reservoir based on petrophysical properties

Numerous previous studies demonstrated the evaluation criteria are based on large amounts of petrophysical property data, and rules are based on collections of empirical statistics to distinguish the cutoffs of conven-

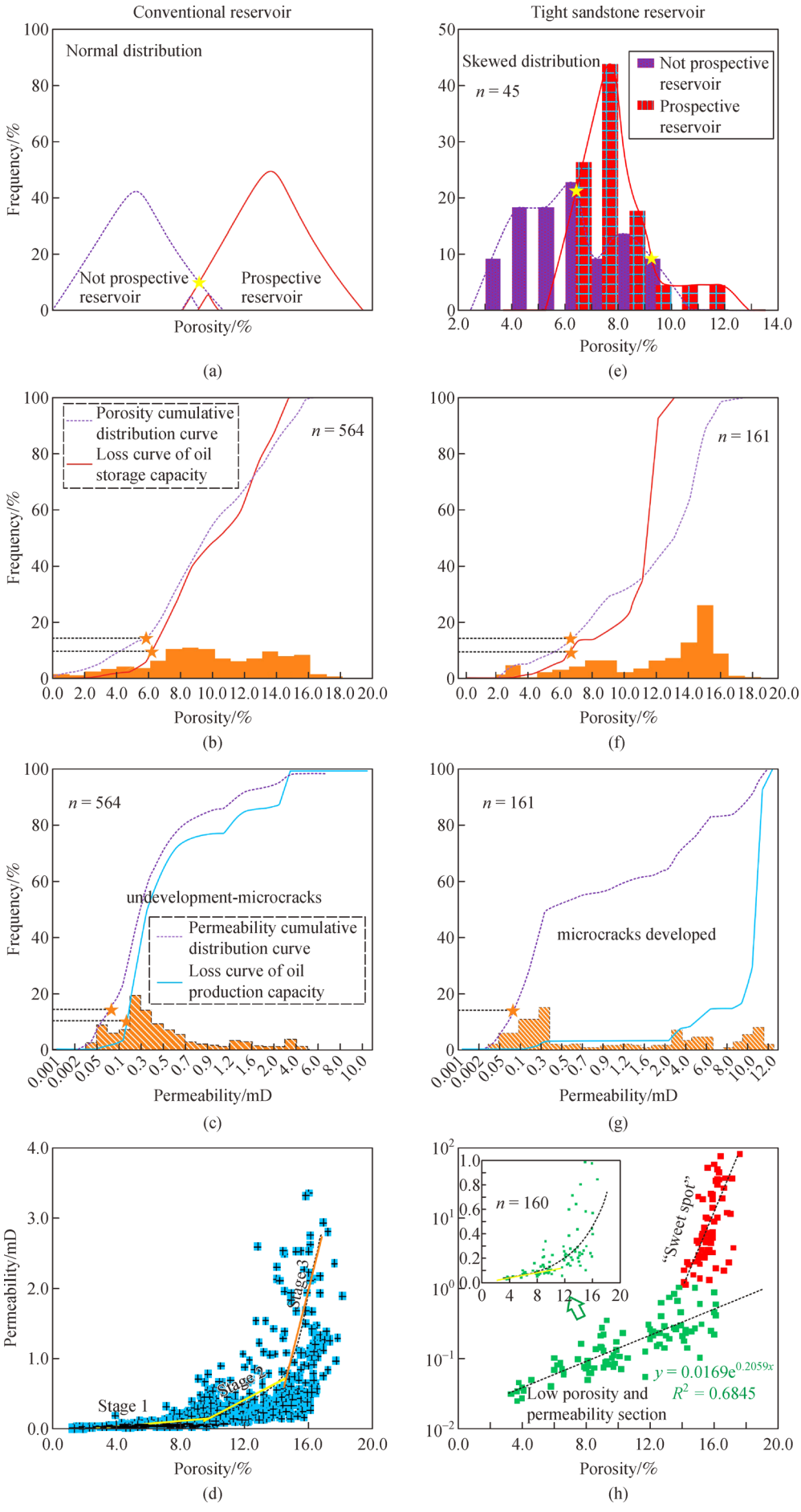


**Fig. 5** Schematic diagram showing the difference of petrophysical property between (a–d) conventional reservoir and (e–h) tight sandstone reservoir (Wan et al., 1999; Wei et al., 2005; Jiao et al., 2009).

tional reservoirs (Hohn, 1989; Wan et al., 1999; Wei et al., 2005; Jiao et al., 2009; Li et al., 2017b; Jing et al., 2020). Traditionally, the physical properties of the conventional reservoir were featured by a normal distribution (Figs. 5(a)–5(c)) and logarithmic correlation (Fig. 5(d)). Owing to the gradual densification of tight sandstone reservoirs, which result in strong heterogeneity and the development of micro-cracks, the development of micro-cracks may enlarge the seepage capacity (Eq. (3)), making the petrophysical properties shown as skewed distribution (Figs. 5(e)–5(g)), and making the relationship between the porosity and permeability more complicated (Fig. 5(h), the relevant petrophysical property data used in this study can be seen in Supplementary data).

$$Q_{Ki} = \frac{K_i \cdot h}{\sum K_i \cdot h_i}, \tag{3}$$

where $Q_{Ki}$: oil production capacity of the $i$th sample, %; $K_i$: permeability of the $i$th sample, mD; $h_i$: length of the $i$th sample, m.

### 4.2 Inapplicability of determining the cut-off of the tight reservoir based on stress sensitivity experiment

In previous studies, some scholars proposed the evaluation criteria based on stress sensitivity experiments (Peng et al., 2009; Cui et al., 2017; Rostami et al., 2019; Shi et al., 2020a). However, the upper limits of permeability of tight sandstone reservoirs are lower than 1 mD, which is lower than the requirements of the industry standard for stress sensitivity experiment (SY/T5358-2002, ≥1 mD). Moreover, tight sandstone reservoirs have undergone intense compaction and gradual densification within the deep-burial condition. As such, the results of stress sensitivity experiments of 13 samples show that with the increase of overburden pressure, permeability and porosity decrease (Fig. 6), and the range within which permeability decreases is greater than those of porosity, which reveals that the permeability is more sensitive to overburden stress than the porosity. Besides, the larger the initial permeability is, the greater the range decreases; while when the initial value is very low, the decrease range is limited. Increasing the pressure only causes little changes in stress, leading to large errors (Fig. 6). Hence, the method based on the stress sensitivity experiment does not recommend for tight sandstone reservoirs.

### 4.3 Redefining the cutoffs of physical properties of tight sandstone reservoirs based on field operations

According to grain-size analysis and oil-bearing occurrence data derived from core observation of the Chang 6, Chang 8 and Chang 9 oil layers, the oil-bearing occurrences of fine- to medium-sandstones are mainly oil

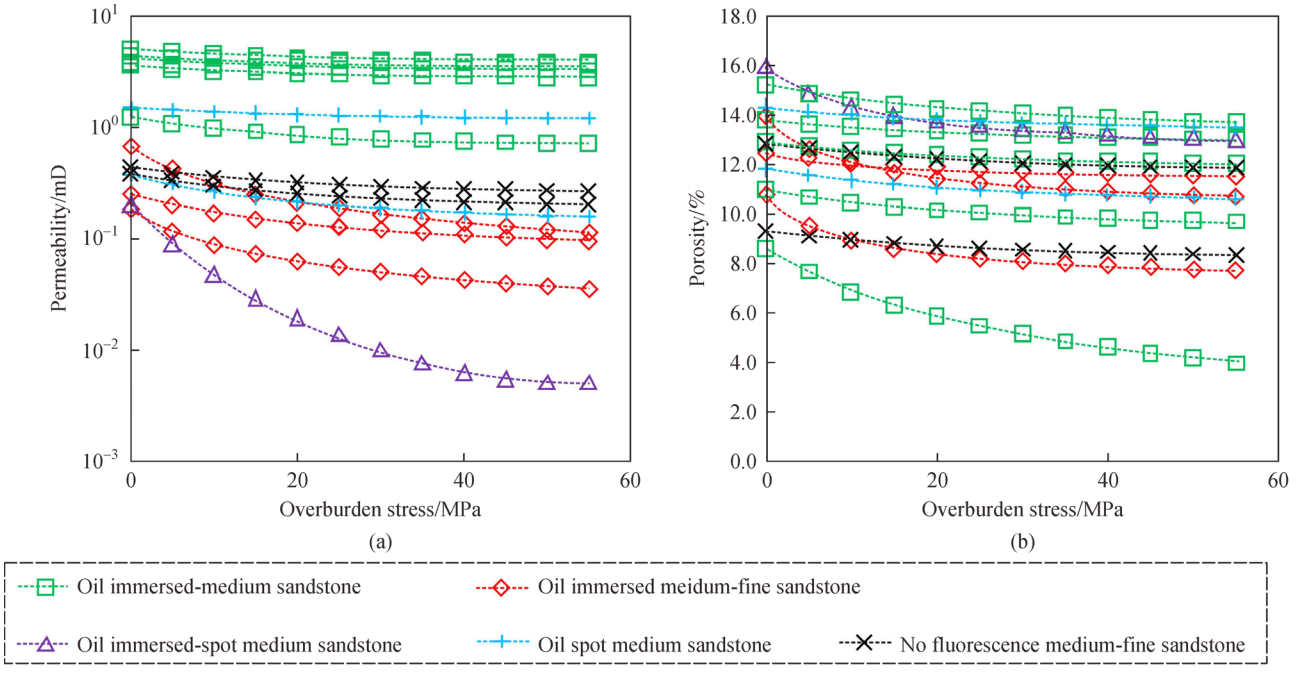


**Fig. 6** Stress sensitivity analysis for the Chang 6, Chang 8 and Chang 9 oil layers in the Zhenjing Block.

spots to oil immersions, while siltstones and argillaceous siltstones and mudstones generally do not show fluorescence. In particular, gritstone is unfavorable for the preservation of crude oil due to its large grain size and small specific surface area (Figs. 7(a)–7(c)). These findings revealed that the lithology of the effective reservoir is fine-medium sandstone. As shown in Figs. 7(d)–7(f), there is a good correlation between the petrophysical properties and the oil-bearing occurrences of the tight sandstone reservoirs. In general, the oil-bearing occurrence of commercial oil flow wells generally reaches the levels of oil traces to oil spots. As shown in Figs. 7(d)–7(f), the cutoffs of the porosity of effective reservoirs in the Chang 6, Chang 8 and Chang 9 oil layers are 8.0%, 3.0%, and 11.5%, and the corresponding permeability are 0.10 mD, 0.20 mD, and 0.20 mD, respectively. The sweet spot, generally is those reservoir rocks that are characterized by relatively high-quality greater than the average values of tight gas sands at a specific depth interval. The oil-bearing occurrences of the "sweet spot" generally reached to oil-spot, and exhibited

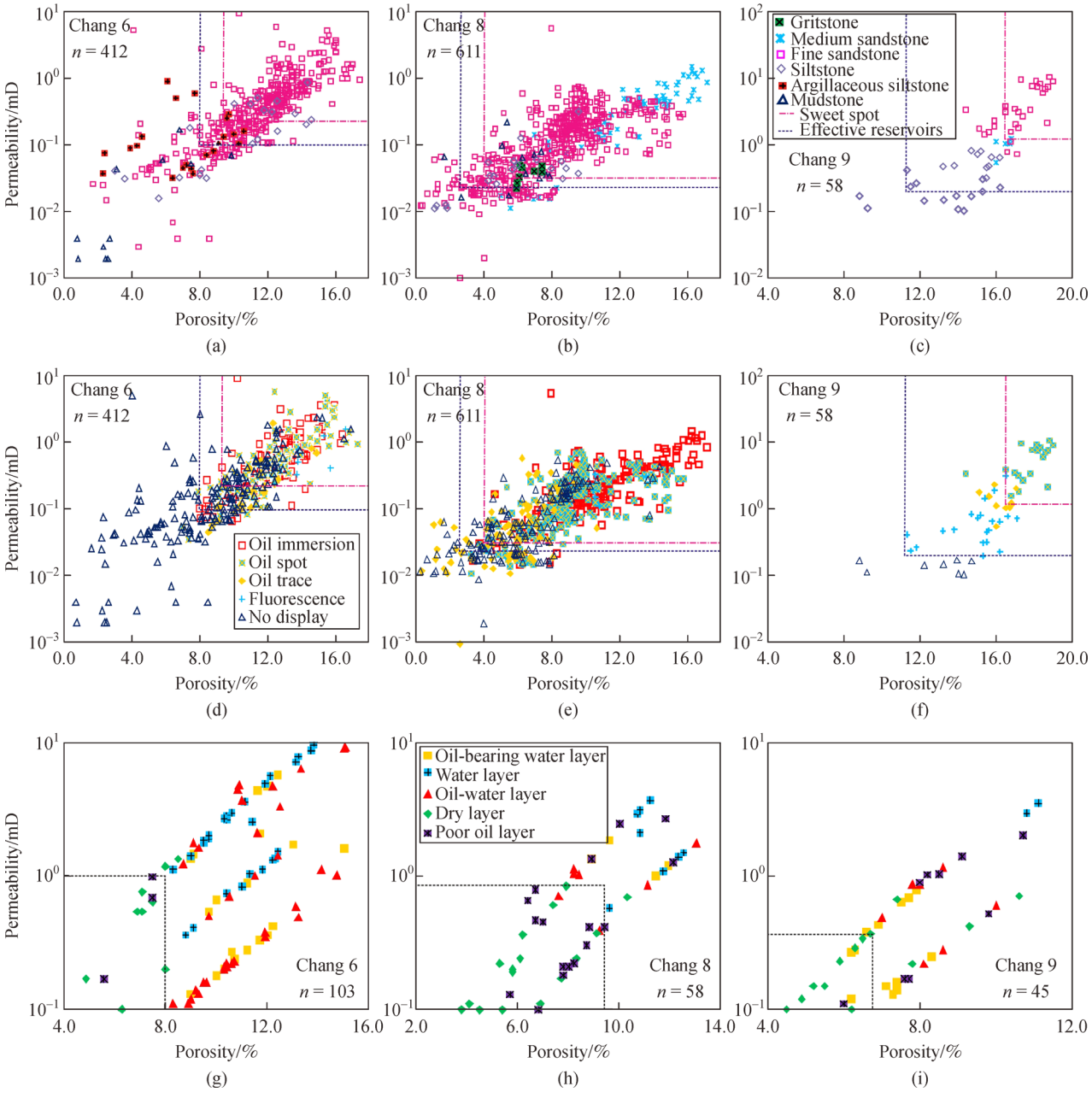


**Fig. 7** Comprehensive determination of the cutoffs of the petrophysical property of the Chang 6, Chang 8 and Chang 9 oil layers using field data.

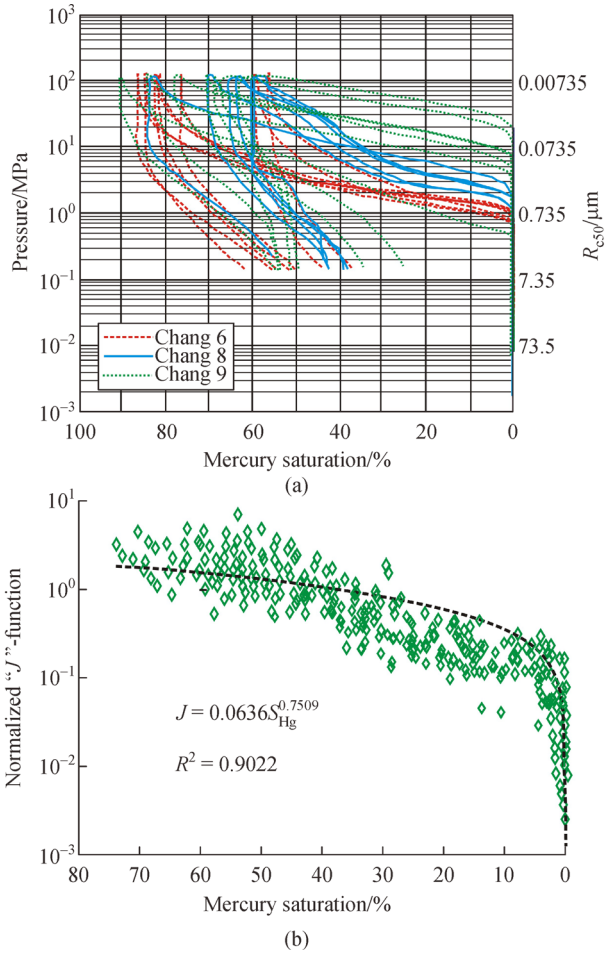


**Fig. 8** (a) Morphology characteristics of mercury injection curves and (b) the cross-plot of mercury saturation versus normalized "*J*'-function of Chang 6, Chang 8 and Chang 9 oil layers in the Zhenjing Block.

commercial exploration potential (Khlaifat et al., 2011; Stabell, 2013; Wang et al., 2020a and 2020b; Zhao et al., 2020). Correspondingly, the cutoffs of "sweet spot" in the Chang 6 and Chang 9 oil layers are 9.0%, 4.0% and 17.0%, 0.3 mD, 0.3 mD and 1.0 mD, respectively.

In this study, wireline well logging interpreted data are also utilized to distinguish the cutoffs of physical properties of the commercial layer (i.e., oil layer, oil-bearing water layer, water layer, and oil-water layer) and non-commercial layer (i.e., dry layer and poor oil layer, Wan et al., 1999; Jiao et al., 2009; Fu et al., 2014). According to the wireline well logging interpreted results of eight wells in the studied area, the cutoffs of the porosity of effective reservoirs in the Chang 6, Chang 8, and Chang 9 oil layers can be considered as 8.0%, 9.5%, and 7.0%, respectively (Figs. 7(g)–7(i)).

### 4.4 Redefining the cutoffs of physical properties of tight sandstone reservoirs based on simulation experiments

#### 4.4.1 High-pressure mercury injection capillary pressure experiment

Results of the MICP test revealed that Chang 6, Chang 8, and Chang 9 have different pore-structure characteristics (Fig. 8(a)). The displacement pressure value of Chang 6, Chang 8, and Chang 9 ranges from 0.78 MPa to 0.96 MPa, 1.00 MPa to 1.62 MPa, and 0.81 MPa to 6.45 MPa, respectively. The median pressure value of Chang 6, Chang 8, and Chang 9 range from 3.65 MPa to 5.44 MPa, 5.43 MPa to 47.52 MPa, and 12.05 MPa to 33.32 MPa, respectively, and the corresponding median radius are 0.01–22.45 μm, 0.20 μm, and 0.01–0.06 μm, respectively. Values of mercury withdrawal efficiency range from 29.21% to 34.16%, 23.80% to 43.64%, and 20.80% to 39.54% for Chang 6, Chang 8, and Chang 9, respectively. Such differences in the characteristics of the pore-throat imply that the cutoffs of the Chang 6, Chang 8, and Chang 9 oil layers are distinct.

In this study, normalized dimensionless Leverett function ("*J*'-function, Eq. (4)) of capillary pressure was applied based on the results of the MICP test (Leverett, 1941; Abedini and Torabi, 2015; Fig. 8b).

$$J(S_{Hg}) = \frac{P_c}{\sigma}\cdot\sqrt{\frac{k}{\varphi}} = 0.086P_c\cdot(k/\varphi)^{-1/2}$$

$$= 0.0636S_{Hg}^{0.7509}, \quad (4)$$

where, $J$: Leverett function; $S_{Hg}$: water saturation, %; $P_c$: capillary pressure, MPa; $\sigma$: surface tension, N/m; $k$: permeability, mD; $\varphi$: porosity, %.

Cumulative permeability method to calculate the minimum flow pore throat radius as seen in Eq. 5. When the cumulative permeability contribution value reaches 99.0%, the corresponding pore throat radius is the minimum flow pore throat radius (Ye et al., 2019). Based on the "*J*'-function, the minimum flow pore throat radius of the Chang 6, Chang 8 and Chang 9 oil layers is 0.017 μm.

$$k = \sum\Delta k_i = \sum\left[\frac{\varphi(2^i-1)r_n^2}{\sum_{i=1}^{n}(2^i-1)r_i^2}\right]\times 100, \quad (5)$$

where, $k$: cumulative permeability, mD; $\Delta k_i$: contribution value of permeability in $i$th interval, mD ; $r_i$: corresponding throat radius of $i$th interval.

Cross-plots of the throat radius versus permeability (Figs. 9(a)–9(c)) proves that the cutoffs of the effective

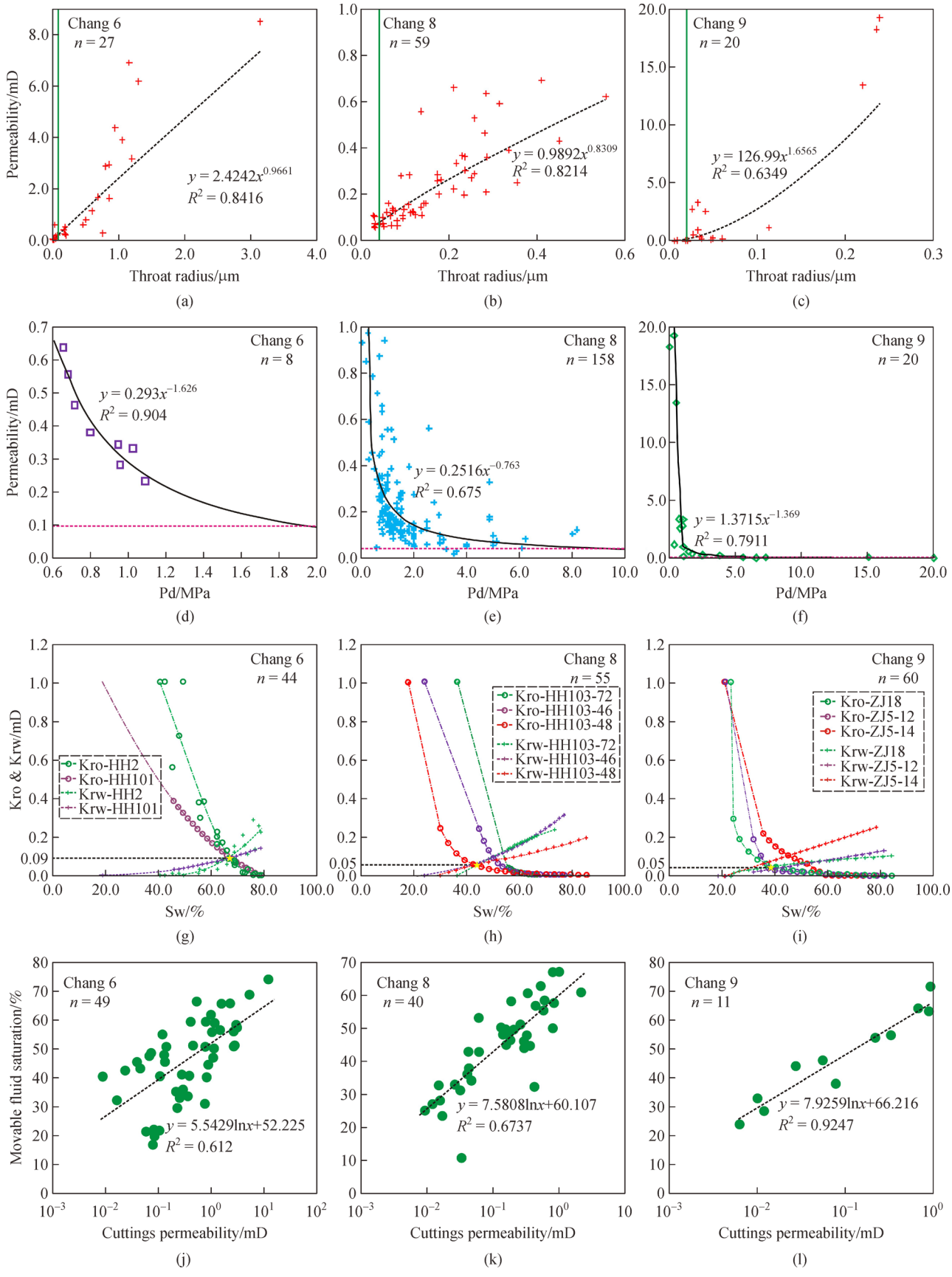


**Fig. 9** Comprehensive determination of the cutoffs of the petrophysical property of the Chang 6, Chang 8 and Chang 9 oil layers through simulation experiments. Notes: The green line shown in Figs. 9(a)–9(c) represent the minimum flow pore throat radius; the red line shown in Figs. 9(d)–9(f) represent the cutoff of permeability of effective reservoir.

reservoir for the Chang 6, Chang 8, and Chang 9 oil layers are 0.05 mD, 0.03 mD, and 0.15 mD, respectively.

As shown in Figs. 9(d)–9(f), there is a good correlation between the displacement pressure versus permeability, manifested as an obvious curve inflection point, which is represented as the cut-off of physical properties of tight sandstone reservoirs (Figs. 8(d)–8(f); Pittman, 1992; Jiao et al., 2009; Fu et al., 2014). When the permeability is less than the inflection point, the values of displacement pressure increase rapidly. And when the permeability is higher than the inflection point, the values of displacement pressure do not change significantly. As shown in Figs. 9(d)–9(f), the cutoffs of permeability of effective reservoirs in the Chang 6, Chang 8, and Chang 9 oil layers are 0.10 mD, 0.05 mD, and 0.10 mD, respectively.

#### 4.4.2 Oil-water relative permeability experiment

As seen in oil-water relative permeability curves, the lower inflection point of the oil phase permeability curve is considered as the cut-off of effective reservoirs (Peng et al., 2009; Cui et al., 2017; Rostami et al., 2019). The inflection point of the oil phase permeability curve approaches from the intersection point of oil and water phase permeability. Therefore, the intersection point can be considered as the cut-off of effective reservoirs (Shi et al., 2020a). As shown in Figs. 8(g)–8(i), the intersections of the oil-water relative permeability curves of eight wells indicated that the cut-off of permeability of effective reservoirs in the Chang 6, Chang 8, and Chang 9 oil layers are 0.09 mD, 0.05 mD, and 0.05 mD, respectively.

#### 4.4.3 Nuclear magnetic resonance experiment

Movable fluid saturation is an important indicator for evaluating the physical properties and determining the cut-off of tight sandstone reservoirs (Zhang et al., 2020). The $T_2$ distributions in the irreducible and movable fluid states can be used to characterize the irreducible and movable fluid micro-distribution, respectively. The $T_2$ distribution in the fluid-saturated state represents the comprehensive response of the irreducible fluid and the movable fluid in the pores. Hence, based on the cut-off standard of saturation of the movable fluid of the Langfang State Key Laboratory ( $>10\%$), the results of a gas displacement test of core samples from seven wells indicated that the cut-off of cutting permeability of Chang 6, Chang 8, and Chang 9 are 0.0824 mD, 0.0347 mD, and 0.0063 mD, and the corresponding movable fluid saturations are 16.98%, 10.80%, and 24.15%, respectively (Figs. 8(j)–8(l)).

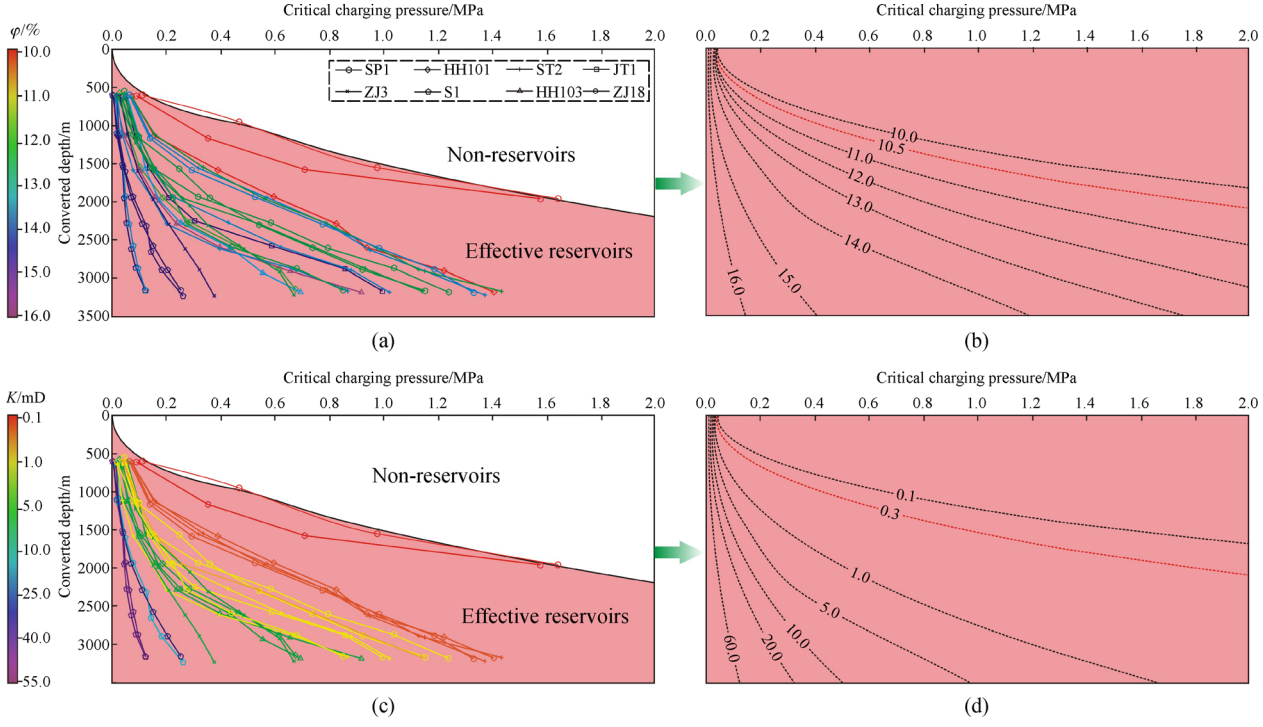


**Fig. 10** Cross-plots of differences in critical charging pressure versus burial depth of the Chang 6, Chang 8 and Chang 9 tight sandstones in the Zhenjing Block.

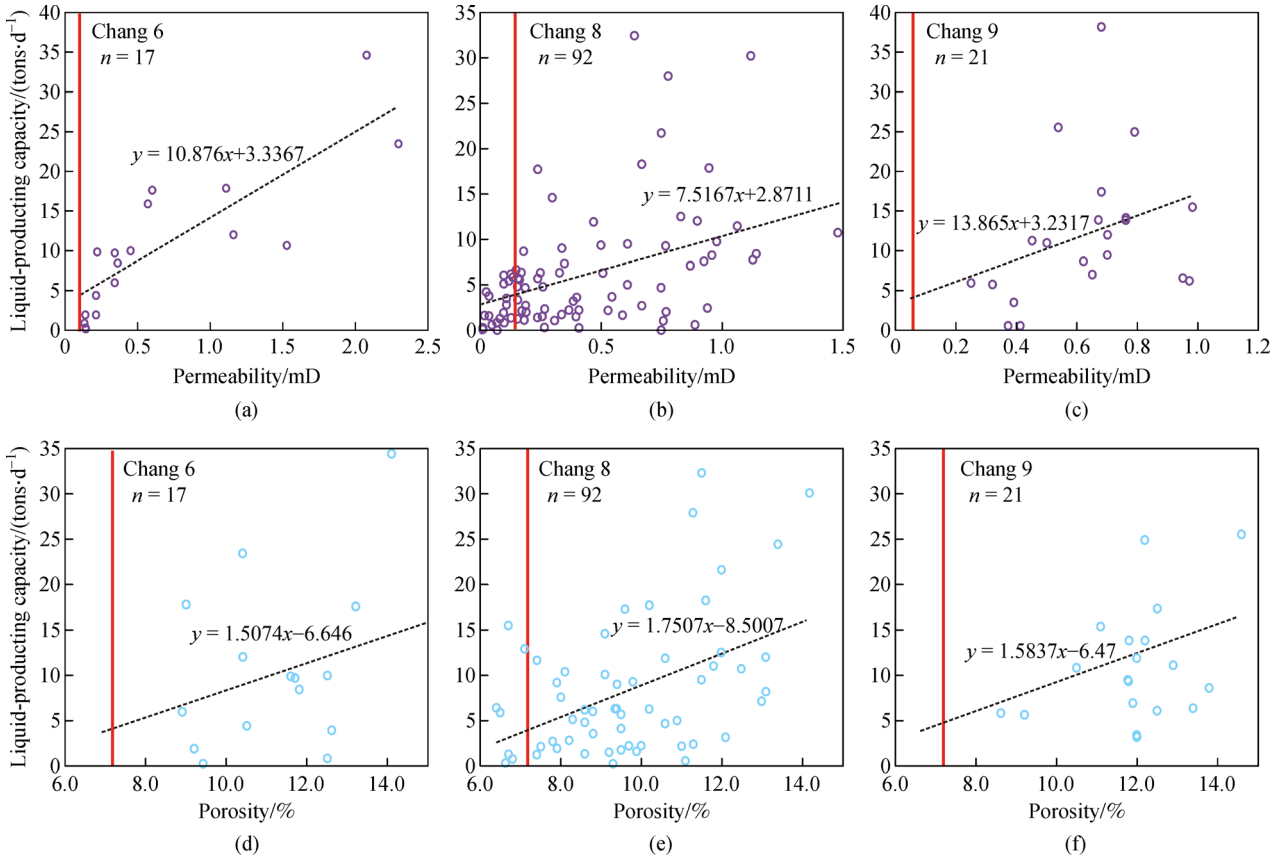


**Fig. 11** Cross-plots showing daily oil yield versus permeability (a–c) and daily oil yield versus porosity (d–f) of the oil-bearing intervals of the Chang 6, Chang 8 and Chang 9 oil layers in the Zhenjing Block. Note: The red line represent the cutoff of permeability and porosity of effective reservoir.

#### 4.4.4 Biaxial pressure simulation experiment

The results of the biaxial pressure simulation experiment demonstrate that most core samples of the Chang 6 oil layer can be injected with oil under high fluid pressure. Except for one sample of the Chang 8 oil layer (well ZJ18-4), in which oil could be injected under high fluid pressure, the other 20 samples could not be injected with oil even at the maximum filling fluid pressure (30 MPa/m) (Fig. 10). The comparison between the filling results and core physical data shows that when the core porosity is less than 10.5% and the permeability is less than 0.34 mD, oil cannot be injected even if the filling pressure is increased to the maximum value. Based on this, the cut-off of porosity of the Chang 6 and Chang 8 oil layers is 10.5%, and the corresponding cut-off of permeability is 0.34 mD.

### 4.5 Assessment of the cutoffs of physical properties of tight sandstone reservoirs by oil testing data

The comprehensive analysis has shown that the average of cutoffs of permeability of the Chang 6, Chang 8, and Chang 9 are 0.08 mD, 0.05 mD, and 0.09 mD, respectively, and the corresponding the average of cutoffs of porosity of the Chang 6, Chang 8, and Chang 9 are 7.9%, 6.4%, and 8.6%, respectively. According to petroleum industry standards of China, when the oil layer is buried at depths of 1000–2000 m, the daily oil yield must be $>1$ ton/d, which corresponds to the industrial oil layer, and when the oil layer is buried at depths of 2000–3000 m, the daily oil yield must be $>3$ tons/d, which also corresponds to the industrial oil layer (SY/T 6293-2008). Figure 11 shows cross-plots of the daily oil yield versus permeability (Figs. 11(a)–11(c)) and daily oil yield versus porosity (Figs. 11(d)–11(f)) of the Chang 6, Chang 8, and Chang 9 oil layers in the Zhenjing Block. When the above values are taken, the minimum daily oil yield of the effective reservoir is $>4$ tons/d, which is consistent with the standard of commercial oil flow of tight sandstone reservoirs.

### 4.6 The effective thickness for Chang 6–Chang 9 oil layers

The Chang 6, Chang 8 and Chang 9 tight sandstones in the Zhenjing Block underwent a complex diagenetic evolution

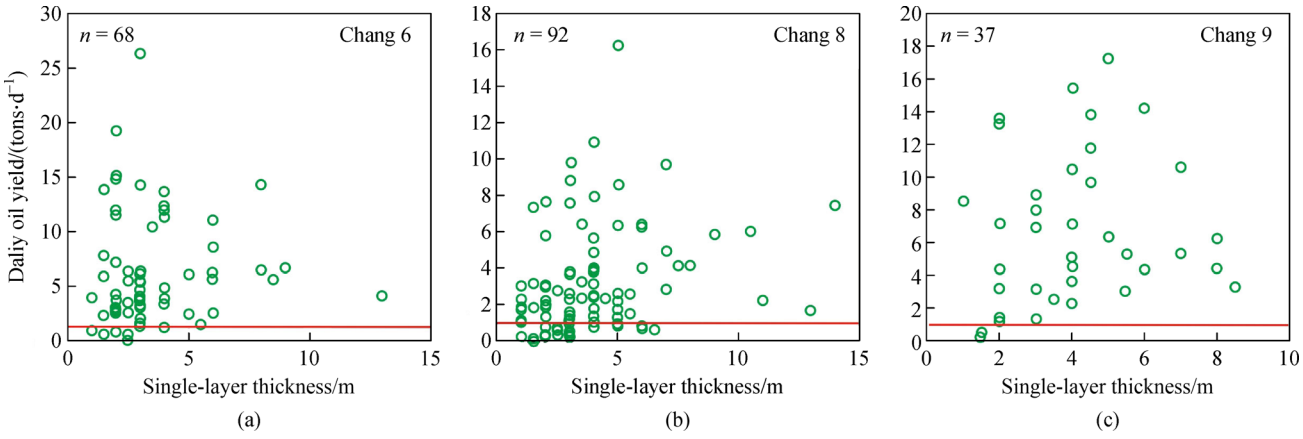


**Fig. 12** Cross-plots showing single-layer thickness versus results of well testing of the (a) Chang 6, (b) Chang 8 and (c) Chang 9 oil layers in the Zhenjing Block. Note: The dark dotted line represent the cutoff of single-layer thickness of effective reservoir.

(Wang et al., 2005 and 2017a; Li et al., 2017a and 2019b; Shi et al., 2019, 2020a and 2020b; Liu et al., 2020b; Yang et al., 2020). However, in a single-layer thick reservoir, primary or secondary pores in the sand body are kept to a greater extent, and the physical properties are usually superior. After a comprehensive comparative analysis of wireline well logging, mud logging, and well testing analyses of the Chang 6, Chang 8, and Chang 9 oil layers, the cut-off of the thickness of single-layer effective reservoirs were found to vary among different layers, and the cut-off of the thickness of single-layer effective sandbodies are approximately 3.0 m, 3.0 m, and 2.0 m, respectively (Fig. 12).

### 4.7 Planar distribution of effective tight sandstone reservoirs and its application to petroleum exploration

As mentioned above, the cut-off of the porosity of effective reservoirs in the Chang 8 oil layer is approximately 6.4% and 0.05 mD, and the corresponding cut-off of the thickness of single-layer effective sand body is approximately 3.0 m. Figures 13(a) and 13(b) show that the majority of commercial oil flow wells and oil flow wells are located in areas with $>10\%$ porosity and $>3$ m thickness of the single-layer sand body. In contrast, many of the drilling wells show dry layers and water layers all located in areas with $<10\%$ porosity and $<3$ m thickness of the single-layer sand body. As shown in Figs. 13(c)–11(d), the commercial oil flow wells, oil flow wells, and oil-water layers all plotted in the congruent areas of $>6.4\%$ porosity, $>0.05$ mD permeability and $>3$ m thickness of the single-layer sand body, the dry wells all plotted in the congruent areas of $<6.4\%$ porosity, $<0.05$ mD permeability and $<3$ m thickness of the single-layer sand body. These results note that the prospective targets are mainly distributed in long-strips in a NE-SW trend. Wherein the areas around wells HH44, ZT1 and HH103 are the major favorable areas.

Determining favorable areas is essential to reserve calculation. In the process of its determination, an effective reservoir thickness is mostly taken as boundary basis. An energy-storage coefficient ($\varphi \cdot h \cdot S_o$, herein, $\varphi$ is porosity, %; $h$ is the thickness of single-layer, m; $S_o$: Oil saturation, %) was taken as the boundary basis to calculate reserves, and its planar distribution map was plotted by means of reservoir prediction (Zhang et al., 2018; Shi et al., 2019; Zhang et al., 2019; Chen et al., 2020). And accordingly, the lithological boundary of effective reservoirs was determined and the favorable areas were delineated. In contrast with the map of the energy-storage coefficient of the Chang 8 oil layer (Fig. 14), the majority of sandbodies in prospective targets were plotted in the area of the energy-storage coefficient $>1.0$.

## 5 Conclusions

In the consideration of the characteristics of complex reservoir quality, non-Darcy flow, strong heterogeneity, and micro-pore throats of tight sandstone reservoirs, some approaches based on field operations and simulation experiments were preferred for comprehensive delineated the cutoffs of tight sandstone reservoirs. The preferred approaches are of profound significance for resource evaluations of tight oil reservoirs and the selection of exploration zones.

The physical property cutoffs of the effective reservoirs of the Chang 6, Chang 8, and Chang 9 oil layers are 7.9%, 6.4%, and 8.6%, respectively, and the cutoffs of the thickness of single-layer effective reservoirs are approximately 3.0 m, 3.0 m, and 2.0 m, respectively.

Using the preferred methods and combining with the cut-off of single-layer thickness, a superimposed map showing the planar distribution of the prospective targets

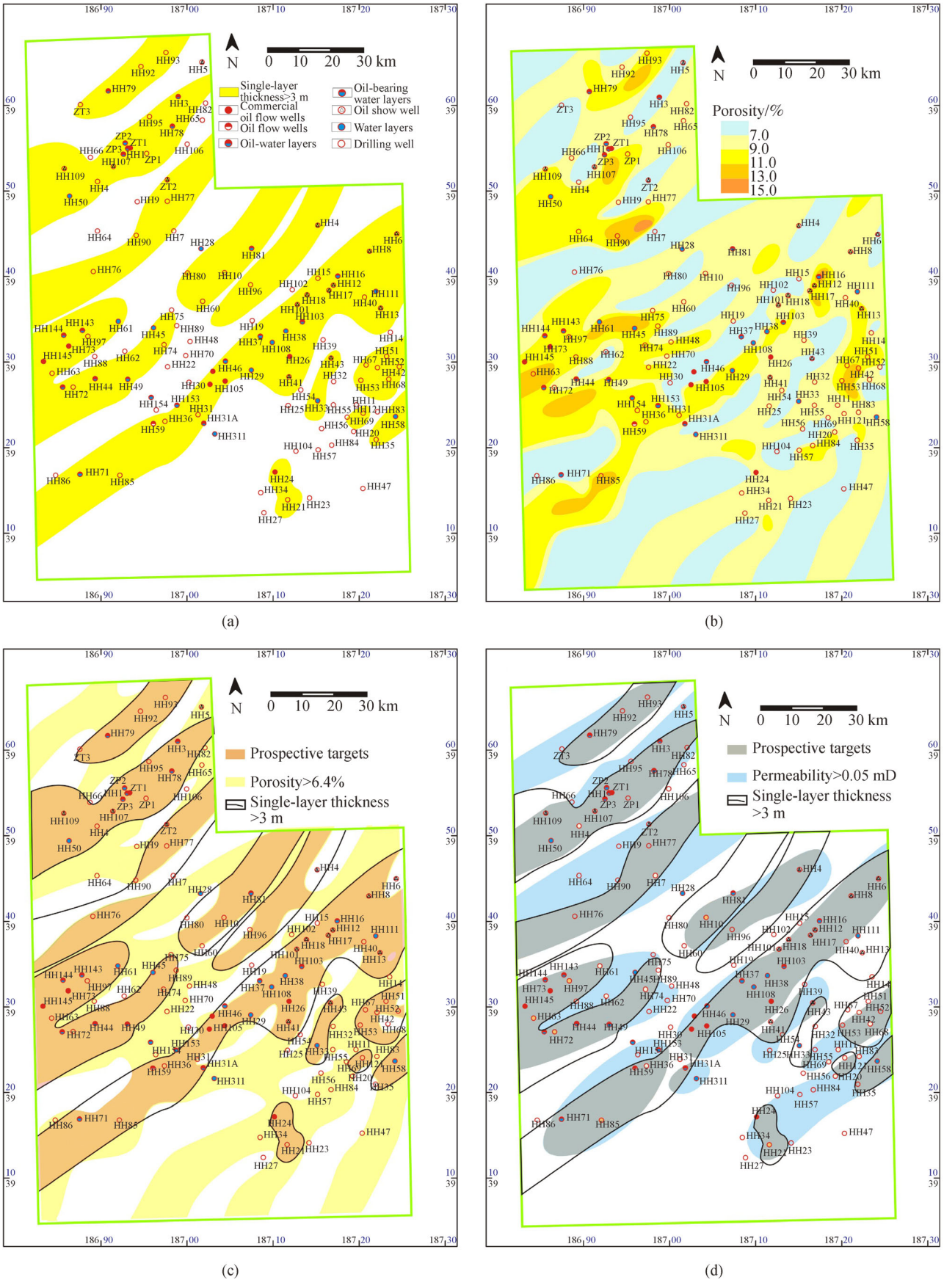


**Fig. 13** (a) Planar distribution map of single-layer thickness > 3 m, (b) isoline map of porosity, (c, d) superimposed map showing prospective targets of the Chang 8 oil layer.

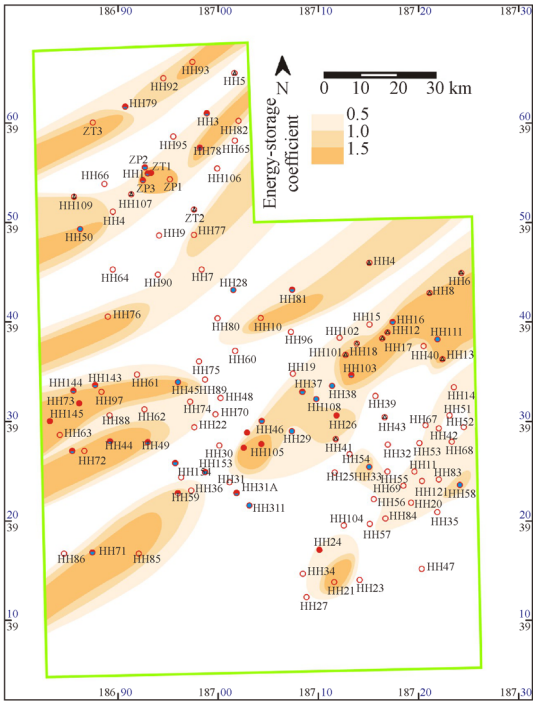


**Fig. 14** Isoline map of the energy-storage coefficient of the Chang 8 oil layer.

was obtained. This map may delineate the effective boundary of prospective targets for petroleum exploration of tight sandstone reservoirs.

**Acknowledgements** This study was supported by the National Natural Science Foundation of China (Grant Nos. 42072172 and 41772120), the Shandong Province Natural Science Fund for Distinguished Young Scholars (No. JQ201311), and the Graduate Scientific and Technological Innovation Project Financially Supported by Shandong University of Science and Technology (No. SDKDYC190313). We thank Shengli Oilfield Company of Sinopec for approving the publication. We also acknowledge the experts of Elsevier Webshop support for its linguistic assistance during the preparation of this manuscript. Three anonymous reviewers and Editorial Office were deeply acknowledged for their critical comments and helpful suggestions, which greatly improved the early version of this manuscript.

**Electronic supplementary material** is available in the online version of this article at http://dx.doi.org/10.1007/s11707-020-0851-z and is accessible for authorized users.

## References

Abedini A, Torabi F (2015). Pore size determination using normalized J-function for different hydraulic flow units. Petroleum, 1(2): 106–111

Adebayo A R, Bageri B S, Jaberi J A, Salin R B (2020). A calibration method for estimating mudcake thickness and porosity using NMR data. J Petrol Sci Eng, 195: 107582

Aguilera R (2014). Flow units: from conventional to tight-gas to shale-gas to tight-oil to shale-oil reservoirs. SPE Reservoir Eval Eng, 17 (02): 190–208

Baytok S, Pranter M J (2013). Fault and fracture distribution within a tight-gas sandstone reservoir: Mesaverde Group, Mamm Creek Field, Piceance Basin, Colorado, USA. Petrol Geosci, 19(3): 203–222

Chen W, Zhao C N, Jia S, Zeng Y Y, He K L, Xu S Y, Yang J, Lin Y, Li Y (2020). Energy-storage coeffcient to determine reservoir boundary: an example from Longwangmiao Formation, GS6 well block, AY gasfeld, Sichuan Basin. Natural Gas Exploration and Development, 43(1): 22–27

Cui H Y, Zhong N N, Li J, Wang D L, Li Z S, Hao A S, Liang F (2017). Study on the lower limits of petrophysical parameters of the Upper Paleozoic tight sandstone gas reservoirs in the Ordos Basin, China. Journal of Natural Gas Geoscience, 2(1): 21–28

Cui J W, Zhu R K, Mao Z G, Li S X (2019). Accumulation of unconventional petroleum resources and their coexistence characteristics in Chang 7 shale formations of Ordos Basin in central China. Front Earth Sci, 13(3): 575–587

Dai J, Ni Y, Wu X (2012). Tight gas in China and its significance in exploration and exploitation. Pet Explor Dev, 39(3): 277–284

David C, Wong T F, Zhu W L, Zhang J (1994). Laboratory measurement of compaction induced permeability change in porous rocks: implications for the generation and maintenance of pore pressure excess in the crust. Pure Appl Geophys, 143(1–3): 425–456

Esmaeili S, Sarma H, Harding T, Maini B (2019). Review of the effect of temperature on oil-water relative permeability in porous rocks of oil reservoirs. Fuel, 237: 91–116

Folk R L, Andrews P B, Lewis D W (1970). Detrital sedimentary rock classification and nomenclature for use in New Zealand. N Z J Geol Geophys, 13(4): 937–968

Fu J H, Luo A X, Zhang N N, Deng X Q, Lv J W, Wu K J, Wang K, Liu L F (2014). Determine lower limit of physical properties of effective reservoirs in Chang 7 oil formation in Ordos Basin. China Petroleum Exploration, 19: 82–88 (in Chinese)

Gies R M (1984). Case history for a major Alberta Deep Basin gas trap: the Cadomin Formation. AAPG Mem, 38: 115–140

Gong Y J, Liu, S B, Zhao M J, Xie H B, Liu K Y (2016). Characterization of micro pore throat radius distribution in tight oil reservoirs by NMR and high pressure mercury injection. Petroleum Geology and Experiment, 38: 389–394

Guo J X, Li Q, Wang W W, Zhang Q, Wang J H, Hou Z T (2017). Diagenetic sequence and genetic mechanism of Silurian tight sandstone reservoirs in the Eastern Tarim Basin, Northwest China. J Earth Sci, 28: 1109–1125

Hu S Y, Zhu R K, Wu S T, Bai B, Yang Z, Cui J W (2018). Exploration and development of continental tight oil in China. Pet Explor Dev, 45 (4): 790–802

Holditch S A (2006). Tight gas sands. J Pet Technol, 58(06): 86–93

Hohn M E (1989). Geostatistics and Petroleum Geology. New York: van Nostrand Reinhold

Jia C Z, Zou C N, Li J Z, Li D, Zheng M (2016). Evaluation criteria, major types, characteristics and resource prospects of tight oil in China. Petroleum Research, 1(1): 1–9

Jiao C H, Xia D D, Wang J, Liu L, Sheng W B, Cheng P T (2009). Methods for determining the petrophysical property cutoffs of extra-low porosity and permeability sandstone reservoirs: an example from

the Xishanyao Formation reservoirs in Yongjin Oilfield. Oil & Gas Geology, 30: 379–383

Jing F T, Luo X, Yang Z, Zhang L J, Li S X, Chen Y, Zeng Y F (2020). Study on the porosity and permeability cutoffs of tight sandstones in shale stratum: case study of Chang 7 Member of the Triassic Yanchang Formation, Ordos Basin. Natural Gas Geoscience, 31: 835–845

Kikani J, Pedrosa Jr O A, (1991). Perturbation analysis of stress-sensitive reservoir. Soc Pet Eng Form Eval, 6

Khlaifat A L, Qutob H, Barakat N (2011). Tight gas sands development is critical to future world energy resources. In: SPE Middle East Unconventional Gas Conference and Exhibition. Society of Petroleum Engineers

Law B E, Curtis J B (2002). Introduction to unconventional petroleum systems. AAPG Bull, 86: 1851–1852

Leverett M C (1941). Capillary behavior in porous solids. Transactions of the AIME, 142, 151–169

Li Y, Chang X C, Yin W, Sun T, Song T (2017a). Quantitative impact of diagenesis on reservoir quality of the Triassic Chang 6 tight oil sandstones, Zhenjing area, Ordos Basin, China. Mar Pet Geol, 86: 1014–1028

Li Y, Chang X C, Yin W, Wang G, Zhang J, Shi B, Zhang J, Mao L (2019a). Quantitative identification of diagenetic facies and controls on reservoir quality for tight sandstones: a case study of the Triassic Chang 9 oil layer, Zhenjing area, Ordos Basin. Mar Pet Geol, 102: 680–694

Li Y, Gao X, Meng S, Wu P, Niu X, Qiao P, Elsworth D (2019b). Diagenetic sequences of continuously deposited tight sandstones in various environments: a case study from upper Paleozoic sandstones in the Linxing area, eastern Ordos basin, China. AAPG Bull, 103(11): 2757–2783

Li Y, Xu W, Wu P, Meng S (2020). Dissolution versus cementation and its role in determining tight sandstone quality: a case study from the Upper Paleozoic in northeastern Ordos Basin. China Journal of Natural Gas Science and Engineering, 78: 103324

Li Y, Yang J, Pan Z, Meng S, Wang K, Niu X (2019c). Unconventional natural gas accumulations in stacked deposits: a discussion of Upper Paleozoic coal-bearing strata in the east margin of the Ordos Basin, China. Acta Geol Sin, 93(1): 111–129

Li P, Zheng M, Bi H, Wu S, Wang X (2017b). Pore throat structure and fractal characteristics of tight oil sandstone: a case study in the Ordos Basin, China. J Petrol Sci Eng, 149: 665–674

Liu H P, Zhao Y C, Luo Y, Xiao G, Meng Y, Zhou S, Shao L (2020a). Origin of the reservoir quality difference between Chang 8 and Chang 9 Member sandstones in the Honghe Oil Field of the Southern Ordos Basin, China. J Petrol Sci Eng, 185: 106668

Liu G D, Sun M L, Zhao Z Y, Wang X, Wu S (2013). Characteristics and accumulation mechanism of tight sandstone gas reservoirs in the Upper Paleozoic, northern Ordos Basin, China. Petrol Sci, 10(4): 442–449

Liu L L, Li Y, Dong H Z, Sun Z Q (2020b). Diagenesis and reservoir quality of Paleocene tight sandstones, Lishui Sag, East China Sea Shelf Basin. Journal of Petroleum ence and Engineering, online, doi:10.1016/j.petrol.2020.107615

Liu Z, Liu J J, Wang W, Pan G F, Wang J, Guo Y R, Zhao J Q (2012a). Experimental analyses on critical conditions of oil charge for low-permeability sandstones: a case study of Xifeng Oilfield, Ordos Basin. Acta Petrol Sin, 33: 996–1002 (in Chinese)

Liu Z, Wang W, Pan G F, Xia L, Zhao S, Zhao J Q (2012b). Experiment analysis of relationship between property and oil injection critical pression of low porosity and permeability sandstone within Chang-8 Member, Zhenjing area of Ordos Basin. Chinese Journal of Geology, 47: 440–453 (in Chinese)

Masoudi P, Arbab B, Mohammadrezaei H (2014). Net pay determination by Dempster rule of combination: case study on Iranian offshore oil felds. J Petrol Sci Eng, 123: 78–83

Masters J A (1979). Deep basin gas trap, western Canada. AAPG Bull, 63: 152–181

Makhloufi Y, Collin P, Bergerat F, Casteleyn L, Claes S, David C, Menendez B, Monna F, Robion P, Sizun J P, Swennen R, Rigollet C (2013). Impact of sedimentology and diagenesis on the petrophysical properties of a tight oolitic carbonate reservoir: the case of the Oolithe Blanche Formation (Bathonian, Paris Basin, France). Mar Pet Geol, 48: 323–340

Pang Y M, Guo X W, Han Z Z, Zhang X H, Zhu X Q, Hou F H, Han C, Song Z G, Xiao G L (2019). Mesozoic–Cenozoic denudation and thermal history in the Central Uplift of the South Yellow Sea basin and the implications for hydrocarbon systems: constraints from the CSDP-2 borehole. Mar Pet Geol, 99: 355–369

Pang Y M, Guo X W, Zhang X H, Zhu X, Hou F, Wen Z, Han Z (2020a). Late Mesozoic and Cenozoic tectono-thermal history and geodynamic implications of the Great Xing'an Range, NE China. J Asian Earth Sci, 189: 104155

Pang Y M, Guo X W, Shi B B, Zhang X, Cai L, Han Z, Chang X, Xiao G (2020b). Hydrocarbon generation evaluation, burial history, and thermal maturity of the Lower Triassic–Silurian organic-rich sedimentary rocks in the Central Uplift of the South Yellow Sea Basin, East Asia. Energy Fuels, 34(4): 4565–4578

Peng B, Lv G X, Wanyan Q Q (2009). Determining lower limit of physical property in low-porosity and low-permeability sandstone reservoirs: an example from the 3rd layer in $P_1s^2$ of Zizhou Gasfield. Natural Gas Technology, 3: 34–36

Pittman E D (1992). Relationship of porosity and permeability to various parameters derived from mercury injection-capillary pressure curves for sandstone. AAPG Bull, 76: 191–198

Qiu L W, Yang S C, Qu C S, Xu N, Gao Q, Zhang X, Liu X, Wang D (2017). A comprehensive porosity prediction model for the Upper Paleozoic tight sandstone reservoir in the Daniudi Gas Field, Ordos Basin. J Earth Sci, 28(6): 1086–1096

Rostami S, Rashidi F, Safari H (2019). Prediction of oil-water relative permeability in sandstone and carbonate reservoir rocks using the CSA-LSSVM algorithm. J Petrol Sci Eng, 173: 170–186

Shi B B, Chang X C, Yin W, Li Y, Mao L (2019). Quantitative evaluation model for tight sandstone reservoirs based on statistical methods—a case study of the Triassic Chang 8 tight sandstones, Zhenjing area, Ordos Basin, China. J Petrol Sci Eng, 173: 601–616

Shi B B, Chang X C, Xu Y D, Mao L, Zhang J, Li Y (2020a). Charging history and fluid evolution for the Carboniferous volcanic reservoirs in the western Chepaizi Uplift of Junggar Basin as determined by fluid inclusions and basin modelling. Geol J, 55(4): 2591–2614

Shi B B, Chang X C, Yin W, Mao L X (2020b). The determination of the lower limits of critical properties for the Chang 8 tight sandstone reservoirs in the Zhenjing Block, Ordos Basin. Acta Sedimentalogica Sinica, 38: 231–243 (in Chinese)

Shi X D, Ai C, Zhan J F, Xiao Q H, Hu C Y (2015). Research of seepage flow law of tight oil reservoir in North Songliao Basin. Advances in Petroleum Exploration and Development, 10: 58–63

Stabell C (2013). Integrated risk, resource and value assessment of unconventional petroleum assets. Nature, 293(5831): 370–374

Tan F, Zhao R, Zhao Y, Pan Z, Li H (2017). A case study: evaluating low-porosity and ultra-low-permeability Triassic reservoir rocks in the Ordos Basin by the integration of logs and core. Petrol Geosci, 23 (4): 454–465

Wan L, Sun Y, Wei G (1999). A new method used to determine the lower limit of the petrophysical parameters for reservoir and its application: a case study on Zhongbu gas field in Ordos Basin. Acta Sedimentologica Sinica, 17: 454–457

Wang E Z, Liu G Y, Pang X Q, Wu Z Y, Li C R, Bai H, Zhang Z H (2020a). Sedimentology, diagenetic evolution, and sweet spot prediction of tight sandstone reservoirs: a case study of the third member of the Upper Paleogene Shahejie Formation, Nanpu Sag, Bohai Bay Basin, China. J Petrol Sci Eng, 186: 106718

Wang G W, Chang X C, Yin W, Li Y, Song T (2017a). Impact of diagenesis on reservoir quality and heterogeneity of the Upper Triassic Chang 8 tight oil sandstones in the Zhenjing area, Ordos Basin, China. Mar Pet Geol, 83: 84–96

Wang G W, Hao F, Chang X C, Lan C, Li P, Zou H (2017b). Quantitative analyses of porosity evolution in tight grainstones: a case study of the Triassic Feixianguan formation in the Jiannan gas field, Sichuan Basin, China. Mar Pet Geol, 86: 259–267

Wang G W, Li P P, Hao F, Zou H, Zhang L, Yu X (2015a). Impact of sedimentology, diagenesis, and solid bitumen on the development of a tight gas grainstone reservoir in the Feixianguan Formation, Jiannan area, China: implications for gas exploration in tight carbonate reservoirs. Mar Pet Geol, 64: 250–265

Wang L, He Y M, Chen H, Meng Z, Wang Z (2019). Experimental investigation of the live oil-water relative permeability and displacement efficiency on Kingfisher waxy oil reservoir. J Petrol Sci Eng, 178: 1029–1043

Wang R F, Chen M Q, Sun W (2008). Classification and evaluation of microscopic-pore structure in the ultra-low permeability sandstone reservoir. Acta Geoscientica Sinica, 2: 213–220

Wang X M, Guo Y R, Fu J H, Liu H Q, Chen Q L, Li T S, Liao J B, Zhang C L (2005). Control factors for forming higher porosity and permeability sandstone reservoirs in Chang 8 member of Yanchang Formation, Ordos Basin. Pet Explor Dev, 32: 35–39

Wang Y, Zhu Y M, Wang H Y, Feng G (2015b). Nanoscale pore morphology and distribution of lacustrine shale reservoirs: examples from the Upper Triassic Yanchang Formation, Ordos Basin. Journal of Energy Chemistry, 24(4): 512–519

Wang Z L, Jiang X W, Pan M, Shi Y M (2020b). Nano-scale pore structure and its multi-fractal characteristics of tight sandstone by $N_2$ adsorption/desorption analyses: a case study of Shihezi Formation from the Sulige Gas Filed, Ordos Basin. China, Minerals, 10(4): 377

Wei X W, Xie J R, Tang D H, Chen H B, Xie B (2005). Methods of determining the matrix petrophysical cut-offs of low porosity and low permeability sandstone reservoir: taking the $J_2s_1$ oil reservoir in LA field in central Sichuan as an example. Natural Gas Industry, 2005, 25 (Suppl. 1): 28–31, 11

Worthington P F, Cosentino L (2005). The role of cut-offs in integrated reservoir studies. SPE Reservoir Eval Eng, 8(4): 276–290

Worthington P F (2008). The application of cut-offs in integrated reservoir studies. SPE Reservoir Eval Eng, 11(6): 968–975

Worthington P F (2010). Net pay-what is it? What does it do? How do we quantify it? How do we use it? SPE Reservoir Eval Eng, 13(5): 812–822

Worthington P F, Majid A A (2014). The use of Net-Pay Concepts in the exploitation of shale-gas deposits. J Petrol Sci Eng, 120: 78–85

Yang H, Li S X, Liu X Y (2013). Characteristics and resource prospects of tight oil and shale oil in Ordos Basin. Acta Petrol Sin, 34: 1–11 (in Chinese)

Yang H, Liang X W, Niu X B, Feng S, You Y (2017). Geological conditions for continental tight oil formation and the main controlling factors for the enrichment: a case of Chang 7 Member, Triassic Yanchang Formation, Ordos Basin, NW China. Pet Explor Dev, 44 (1): 11–19

Yang S, Bao Z, Wang N, Qu X, Lin Y, Shen J, Awan R S (2020). Diagenetic evolution and its impact on reservoir quality of tight sandstones: a case study of the Triassic Chang 6 Member, Ordos Basin, northwest China. Mar Pet Geol, 117: 104360

Ye C, Deng P, He R X, Li C H, Liu Q J (2019). Determining the lower limit of physical property in tight sandstone reservoirs: an example from Shanxi 1 Member, Longdong area, Ordos Basin. Natural Gas Exploration and Development, 42: 32–37 (in Chinese)

Zhang H, Hu W W, Liu Q, Shi J T, Shi C Y, Song Z J (2019). Study on flow unit distribution of the low permeability gas reservoir in the 2nd Member, Shanxi Formation, Lower Permian, in Ordos Basin. Geological Review, 65(6): 1541–1548 (in Chinese)

Zhang P F, Lu S F, Li J Q, Chang X (2020). 1D and 2D nuclear magnetic resonance (NMR) relaxation behaviors of protons in clays, kerogen and oil-bearing shale rocks. Mar Pet Geol, 114: 104210

Zhao W, Zhang T, Jia C Z, Li X F, Wu K L, He M X (2020). Numerical simulation on natural gas migration and accumulation in sweet spots of tight reservoir. J Nat Gas Sci Eng, 81: 103454

Zhang T, Li X F, Wang Z X, Yan Y K, Qiao X Y, Ma C, Lei K Y, Tang P Z, Feng D, Zhao W (2018). Efficient mobilization method of stereoscopic well pattern in low-permeability complex superimposed tight reservoir: a case study of Yan'an gasfield. Acta Petrol Sin, 39 (11): 1279–1291

Zheng D Y, Pang X Q, Zhou L M, You X C, Liu X H, Guo F X, Li W (2020). Critical conditions of tight oil charging and determination of the lower limits of petrophysical properties for effective tight reservoirs: a case study from the Fengcheng Formation in the Fengcheng area, Junggar Basin. J Petrol Sci Eng, 190: 107135

Zhou Y, Ji Y L, Xu L M, Che S, Niu X, Wan L, Zhou Y, Li Z, You Y (2016). Controls on reservoir heterogeneity of tight sand oil reservoirs in Upper Triassic Yanchang Formation in Longdong Area, southwest Ordos Basin, China: implications for reservoir quality prediction and oil accumulation. Mar Pet Geol, 78: 110–135

Zou C N, Tao S Z, Zhang X, He D, Zhou C, Gao X (2009). Geologic characteristics, controlling factors and hydrocarbon accumulation mechanisms of China's Large Gas Provinces of low porosity and permeability. Sci China Earth Sci, 52(8): 1068–1090

Zou C N, Zhu R K, Liu K Y, Su L, Bai B, Zhang X, Yuan X, Wang J (2012a). Tight gas sandstone reservoirs in China: characteristics and recognition criteria. J Petrol Sci Eng, 88–89: 82–91

Zou C N, Zhu R K, Wu S, Yang Z, Tao S, Yuan X, Hou L, Yang H, Xu C, Li D (2012b). Types, characteristics, genesis and prospects of conventional and unconventional hydrocarbon accumulations: taking tight oil and tight gas in China as an instance. Acta Petrol Sin, 33: 173–187